

**The Influence of Sodium and Potassium Dynamics on Excitability,
Seizures, and the Stability of Persistent States: I. Single Neuron
Dynamics.**

John R. Cressman Jr.^{1*}, Ghanim Ullah², Jokubas Ziburkus³, Steven J. Schiff^{2, 4}, and Ernest Barreto¹

¹ Department of Physics & Astronomy and The Krasnow Institute for Advanced Study, George Mason University, Fairfax, VA, 22030, USA, ² Center for Neural Engineering, Department of Engineering Science and Mechanics, The Pennsylvania State University, University Park, PA, 16802, USA, ³ Department of Biology and Biochemistry, The University of Houston, Houston, TX, 77204, USA, and ⁴ Departments of Neurosurgery and Physics, The Pennsylvania State University, University Park, PA, 16802, USA.

* Corresponding Author

John R. Cressman Jr.,
Krasnow Institute for Advanced Study,
Mail Stop 2A1,
George Mason University,
Fairfax, VA, 22030, USA
Email: jcressma@gmu.edu
Voice: (703) 993 9643
Fax: (703) 993 1269

ABSTRACT

In these companion papers, we study how the interrelated dynamics of sodium and potassium affect the excitability of neurons, the occurrence of seizures, and the stability of persistent states of activity. We seek to study these dynamics with respect to the following compartments: neurons, glia, and extracellular space. We are particularly interested in the slower time-scale dynamics that determine overall excitability, and set the stage for transient episodes of persistent oscillations or seizures. In this first of two companion papers, we construct a mathematical model consisting of a single conductance-based neuron together with intra- and extracellular ion concentration dynamics. We formulate a reduction of this model that permits a detailed bifurcation analysis, and show that the reduced model is a reasonable approximation of the full model's dynamics. We find that the competition between intrinsic neuronal currents, sodium-potassium pumps, and glia-mediated diffusion can produce very slow and large amplitude oscillations in ion concentrations similar to what is seen physiologically in seizure dynamics. Using the reduced model, we identify the dynamical mechanisms that give rise to these phenomena. These models reveal several experimentally testable predictions. Our work emphasizes the critical role of ion concentration homeostasis in the proper functioning of neurons, and points to important fundamental processes that may underlie pathological states such as epilepsy.

Keywords: Potassium dynamics; bifurcation; glia; seizures; instabilities

INTRODUCTION

The Hodgkin-Huxley equations have played a vital role in our theoretical understanding of various behaviors seen in neuronal studies both at single cell and network levels. However, use of these equations often assumes that the intra- and extracellular ion concentrations of sodium and potassium are constant. While this may be a reasonable assumption for isolated single cells, its validity in other cases, especially in mammalian brain, is subject to debate. In mammalian brain the intrinsic excitability of neuronal networks depends on the reversal potentials for various ion currents. The reversal potentials in turn depend on extra- and intracellular concentrations of the

relevant ions. Extracellular potassium concentration ($[K]_o$) and intracellular sodium concentration ($[Na]_i$), for example, accumulate during sustained neuronal activity (Amzica et al., 2002; Heinemann et al., 1977; Moody et al., 1974; Ransom et al., 2000). Increasing $[K]_o$ and $[Na]_i$ modulate the neuronal excitability in competing fashion as the increase in potassium raises its reversal and thus the resting potential, and the depleted sodium gradient causes a lower sodium reversal and thus less potential to drive sodium into the cell. The relatively small extracellular space and weak sodium conductances at normal resting potential cause changes in $[K]_o$ to have a greater effect over neuronal behavior than changes in the sodium concentrations. This overall increase in excitability can cause spontaneous neuronal activity (Mcbain, 1994; Rutecki et al., 1985; Traynelis and Dingledine, 1988). For the most part, studies investigating normal brain states have focused on the intrinsic properties of neurons as well as their collective behavior in the networks they form. Although some studies have investigated the role that the extracellular micro-environment play in pathological behavior (Bazhenov et al., 2004; Kager et al., 2000; Somjen et al., 2004; Park and Durand, 2006), little has been done to investigate the cellular control of micro-environmental factors as a means to modulate neuronal response in a microdomain (Park and Durand, 2006).

The most detailed and sophisticated functions of the brain involve precisely organized neuronal firing. These dynamics however, live on a background of relatively slow behavior. Slow modulations, induced by neuromodulators, synaptic plasticity, and other factors changing the neuronal micro-environment can have dramatic effects on the possible dynamics which are displayed by individual cells and networks of cells. Given the importance of the neuronal micro-environment for single cell or network dynamics, a mathematical model incorporating the variable ion concentrations would be very informative. It is very important to have a framework where one can investigate the ranges of variation in the extra- and intracellular ionic concentrations and variety of neuronal behaviors observed as consequences of these variations.

In this first of two companion papers, we show that the interrelated dynamics of sodium and potassium affect the excitability of neurons, the occurrence of seizures, and the stability of persistent states of activity. Since modest increases in $[K]_o$ are known to produce more excitable neurons, it is crucial to understand the behavior of concentration

dynamics as a mechanism for prolonging and perhaps governing seizure behavior. Using the major mechanisms responsible for the upkeep of the cellular micro-environment including pumps, diffusion, glial buffering, cotransporters and channels, we mathematically model a conductance based single neuron embedded within an extracellular space and glial compartments. We formulate a reduction of this model that permits a detailed analytical bifurcation analysis of such dynamics, and show that the reduced model is a reasonable approximation of the full model's qualitative dynamics. The effects of potassium dynamics on the behavior of the neuronal networks will be addressed in the companion article (Ullah et al., Submitted).

METHODS

1. Full model

Our full model consists of one single-compartment conductance-based neuron containing sodium, potassium, calcium-gated potassium, and leak currents, augmented with dynamic variables representing the intracellular sodium and extracellular potassium concentrations. These ion concentrations are affected by the ionic currents listed above, as well as a sodium-potassium pump current, a glial current, and potassium diffusion. Finally, the concentrations are coupled to the membrane voltage equations via the Nernst reversal potentials.

The conductance-based neuron is modeled as follows:

$$\begin{aligned}
 C \frac{dV}{dt} &= I_{Na} + I_K + I_L \\
 I_{Na} &= -g_{Na} [m_{\infty}(V)]^3 h (V - V_{Na}) \\
 I_K &= -\left(g_K n^4 + \frac{g_{AHP} [Ca]_i}{1 + [Ca]_i} \right) (V - V_K) \\
 I_L &= -g_{KL} (V - V_K) - g_{NaL} (V - V_{Na}) - g_{CIL} (V - V_{Cl}) \\
 \frac{dq}{dt} &= \phi [\alpha_q(V)(1 - q) - \beta_q(V)q], \quad q = n, h \\
 \frac{d[Ca]_i}{dt} &= -0.002 g_{Ca} (V - V_{Ca}) / \{1 + \exp(-(V + 25) / 2.5)\} - [Ca]_i / 80
 \end{aligned} \tag{1}$$

The supporting equations are listed below.

$$\begin{aligned}
m_{\infty}(V) &= \alpha_m(V)/(\alpha_m(V) + \beta_m(V)) \\
\alpha_m(V) &= 0.1(V + 30)/[1 - \exp(-0.1(V + 30))] \\
\beta_m(V) &= 4 \exp(-(V + 55)/18) \\
\alpha_n(V) &= 0.01(V + 34)/[1 - \exp(-0.1(V + 34))] \\
\beta_n(V) &= 0.125 \exp(-(V + 44)/80) \\
\alpha_h(V) &= 0.07 \exp(-(V + 44)/20) \\
\beta_h(V) &= 1/[1 + \exp(-0.1(V + 14))]
\end{aligned}$$

We use leak currents similar to those used by (Kager et al., 2000). The gating variable m is assumed to be fast compared to the voltage change; we therefore assume it reaches its equilibrium value m_{∞} immediately (Pinsky and Rinzel, 1994). Finally, the active internal calcium concentration is only used in conjunction with the calcium-gated potassium current in order to model the adaptation seen in many excitatory cells (Mason and Larkman, 1990; Wang, 1998).

The meanings and values of various parameters and variables used in this paper are given in Table 1.

The potassium concentration in the interstitial volume surrounding each cell was continuously updated based on K^+ currents across the neuronal membrane, Na^+K^+ pumps, uptake by the glial network surrounding the neurons and lateral diffusion of K^+ within the extracellular space. The slow K^+ dynamics is modeled with the following equation

$$\frac{d[K]_o}{dt} = 0.33I_K - 2\beta I_{pump} - I_{glia} - I_{diff} \quad (2a)$$

The factor $0.33\text{mM}\cdot\text{cm}^2/\mu\text{coul}$ converts current density to rate-of-change of concentration (see Appendix A) and the factor β corrects for the volume fraction between the interior of the cell and extracellular space when calculating the concentration change and is based on (Mazel et al., 1998; McBain et al., 1990; Somjen 2004).

The sodium-potassium pump is modeled as a product of sigmoidal functions as follows:

$$I_{pump} = \left(\frac{\rho}{1.0 + \exp((25.0 - [Na]_i) / 3.0)} \right) \left(\frac{1.0}{1.0 + \exp(8.0 - [K]_o)} \right).$$

This function is graphed in Fig.1. Normal resting conditions are attained when $\rho = 1.25\text{mM/sec}$. Each term saturates for high values of internal sodium and external potassium, respectively. More biophysically realistic models of pumps, such as those in (Lauger, 1991) produce substantially similar results.

Glial effects are modeled by:

$$I_{glia} = \frac{G_{glia}}{1.0 + \exp((18 - [K]_o) / 2.5)}.$$

This equation models the capacity of glial cells to remove excess potassium from the extracellular space. A similar but more biophysical approach was used in (Kager et al., 2000). Normal conditions correspond to $G_{glia} = 66\text{mM/sec}$, and $[K]_o = 4.0\text{mM}$.

The diffusion current of potassium away from the local extracellular micro-environment is

$$I_{diff} = \varepsilon([K]_o - k_{o,\infty}).$$

$k_{o,\infty}$ is the concentration of potassium in the largest nearby reservoir – either the bath solution in a slice preparation, or the vasculature in the intact brain. For normal conditions, we use $k_{o,\infty} = 4.0$. The diffusion constant ε , obtained from Fick's law, is $\varepsilon = 2D / \Delta x^2$, where we use $D = 2.5 \times 10^{-6} \text{cm}^2/\text{sec}$ for K^+ in water (Fisher et al., 1976) and estimate $\Delta x \approx 20 \mu\text{m}$ for intact brain reflecting the average distance between capillaries (Scharer, 1944); thus $\varepsilon = 1.2\text{Hz}$. The combined effect of the glial current and diffusion are displayed in Fig.2.

To complete the description of the potassium concentration dynamics, we make the assumption that the flow of Na^+ into the cell is compensated by flow of K^+ out of the cell. Then $[K]_i$ can be approximated by

$$[K]_i = 140.0\text{mM} + (18.0\text{mM} - [Na]_i) \quad (2b)$$

where 140.0 mM and 18.0 mM reflect normal resting $[K]_i$ and $[Na]_i$ respectively. The limitations of this approximation will be addressed in the discussion section.

The equations modeling the dynamics intra- and extracellular sodium dynamics are:

$$\frac{d[Na]_i}{dt} = 0.33 \frac{I_{Na}}{\beta} - 3I_{pump} \quad (3a)$$

$$[Na]_o = 144.0mM - \beta([Na]_i - 18.0mM) \quad (3b)$$

In equation (3b) we assume that the total amount of sodium is conserved, and hence only one differential equation for sodium is needed. Here, 144.0mM is the sodium concentration outside the cell under normal resting conditions for a mammalian neuron.

Finally, the reversal potentials appearing in equation (1) are obtained from the ion concentrations via the Nernst equation

$$V_{Na} = 26.64 \ln \left(\frac{[Na]_o}{[Na]_i} \right)$$

$$V_K = 26.64 \ln \left(\frac{[K]_o}{[K]_i} \right)$$

$$V_{Cl} = 26.64 \ln \left(\frac{[Cl]_i}{[Cl]_o} \right).$$

With the leak conductances listed above, the chloride concentrations were fixed at $[Cl]_i = 6.0mM$ and $[Cl]_o = 130mM$.

Thus, the dynamic variables of the full model are V , n , h , $[Ca]_i$, $[K]_o$, and $[Na]_i$. In the results section, we will be interested in varying the parameters G_{glia} , ε , $k_{o,\infty}$, and ρ . We will present our results in terms of parameters normalized by their normal values, for example, $\bar{G}_{glia} = G_{glia} / G_{glia,normal}$, where the overbar indicates the normalized parameter.

2. Reduced model

In order to more effectively study the bifurcation structure of the model presented above, we formulate a reduction by eliminating the fast-time-scale spiking behavior in favor of the slower ion concentration dynamics. This is accomplished by replacing the entire Hodgkin-Huxley mechanism with empirical fits to time-averaged ion currents. Using the membrane conductances from the full model, we fix the external and internal sodium and potassium concentration ratios and allow the model cell to attain its

asymptotic dynamical state, which may be an equilibrium or a limit cycle (spiking). Then, the sodium and potassium membrane currents are time-averaged over one second. These data were fit to products of sigmoidal functions of the sodium and potassium concentration ratios, resulting in the infinite time functions

$I_{Na\infty} \left([Na]_i / [Na]_o, [K]_o / [K]_i \right)$ and $I_{K\infty} \left([Na]_i / [Na]_o, [K]_o / [K]_i \right)$. Details are available in Appendix A. $I_{K\infty}$ is shown in Fig.3a. $I_{Na\infty}$ (not shown) is nearly identical to $I_{K\infty}$, differing significantly only near normal resting concentration ratios due to differences in the sodium and potassium leak currents. Fig.3b shows the same data (the infinite-time potassium currents shown above), replotted after equations (2b) and (3b) were used to express $I_{K\infty}$ as a function of $[K]_o$ and $[Na]_i$ only.

Thus, our reduced model consists of equations (2) and (3), with I_{Na} and I_K replaced with the empirical fits described above (see Appendix A for additional details).

RESULTS

In an experimental slice preparation, an easily-performed experimental manipulation is to change the potassium concentration in the bathing solution. Such preparations have been used to study epilepsy (Jensen and Yaari, 1997; Traynelis and Dingledine, 1988; Gluckman, et al. 2001). At normal concentrations (~4mM), normal resting potential is maintained. However, at higher concentrations (8mM, for example) bursts and seizure-like events occur spontaneously.

We begin discussing the dynamics of our models by considering a similar manipulation, corresponding to varying the normalized parameter $\bar{k}_{o,\infty}$. In the full model, setting $\bar{k}_{o,\infty} = 2.0$ (i.e., doubling the normal concentration of potassium in the bath solution) leads to spontaneously-occurring prolonged periods of rapid firing, as illustrated in the top trace of Fig.4. Each event lasts on the order of several tens of seconds and consists of many spikes, each of which occurs on the order of 0.001 seconds. Thus, the full model contains dynamics on at least two distinct time scales that are separated by four orders of magnitude: fast spiking from the Hodgkin-Huxley mechanism, and a slow overall modulation. The solid traces in the middle and bottom panels show that this slow

modulation corresponds to slow periodic behavior in the sodium and potassium ion concentrations, respectively.

Our reduced model was constructed in order to remove the fast Hodgkin-Huxley spiking mechanism and focus attention on the slow dynamics of the ionic concentrations. The dashed traces in the middle and bottom panels of Fig.4 show the sodium and potassium ion concentrations obtained from the reduced model for the same parameters used above. Although these traces are not identical to those of the full model, it is evident that the reduced model captures the qualitative behavior of the ion concentrations quite well. These concentrations act as slowly-changing parameters that modulate the fast spiking behavior of the neuron.

The separation of time scales achieved by our model reduction is similar in spirit to that of Rinzel and Ermentrout (1989) (see also Kepler, et al., 1992), and yields a model that is amenable to numerical bifurcation analysis. Knowledge of the bifurcations structure informs us about the dynamical mechanisms that underlie the full model. Our main results in this paper consist of identifying bifurcations in the reduced model and analyzing their implications for the behavior of the full model.

For example, Fig.5 shows a bifurcation diagram obtained using the reduced model. This diagram plots the minimum and maximum asymptotic values of the extracellular potassium concentration $[K]_o$ versus a range of values of the reservoir's normalized potassium concentration $\bar{k}_{o,\infty}$. For low values of this parameter, $[K]_o$ is observed to settle at a stable equilibrium that represents resting state behavior in the neuron. The value of $[K]_o$ corresponding to this equilibrium increases with $\bar{k}_{o,\infty}$ until the equilibrium loses stability via a subcritical Hopf bifurcation at $\bar{k}_{o,\infty} \approx 1.9$. At this point, an unstable periodic orbit collides with the equilibrium, and both disappear. $[K]_o$ is subsequently attracted to a large-amplitude stable periodic orbit. The stable and unstable periodic orbits involved in this scenario appear via a saddle-node bifurcation at a parameter value that is extremely close to that of the Hopf bifurcation. The abruptness of this transition is due to the well-known "canard" mechanism (Dumortier and Roussarie, 1996). Thus, large-amplitude periodic fluctuations in $[K]_o$ appear abruptly at a saddle-

node bifurcation. These oscillations persist as $\bar{k}_{o,\infty}$ is increased until the same sequence of bifurcations occurs in the opposite order at $\bar{k}_{o,\infty} \approx 2.13$. At this higher value of $\bar{k}_{o,\infty}$, the unstable equilibrium undergoes a subcritical Hopf bifurcation, becoming stable and giving rise to an unstable periodic orbit whose amplitude quickly rises with increasing $\bar{k}_{o,\infty}$. This orbit then collides with the stable periodic orbit at $\bar{k}_{o,\infty} \approx 2.15$ where both orbits disappear in a saddle-node bifurcation of limit cycles, and the periodic behavior of $[K]_o$ is thus terminated.

In order to examine the boundaries of the periodic solutions described above with respect to pump strength $\bar{\rho}$, the diffusion coefficient $\bar{\varepsilon}$, and glial buffering strength \bar{G}_{glia} , we constructed the bifurcation diagrams shown in Fig.6. First, we fixed all parameters at their normal resting values except $\bar{k}_{o,\infty}$, which we set to 2 in order to obtain the oscillatory behavior discussed above. We then separately varied $\bar{\rho}$, $\bar{\varepsilon}$, and \bar{G}_{glia} away from their normal resting values. If $\bar{\rho}$ and $\bar{\varepsilon}$ are increased from their nominal values of 1 (Fig.6a, b), we see that the oscillatory behavior terminates in a manner similar to that described above; that is, an unstable periodic orbit appears via a subcritical Hopf bifurcation which grows until it collides with and annihilates the stable periodic solution at a saddle-node bifurcation of limit cycles. The same scenario applies as these parameters are decreased, with a canard mechanism similar to that described above, so that the Hopf and the saddle-node bifurcations on the left side of the diagrams occur in extremely narrow intervals of the parameter. The situation is reversed for the glial strength \bar{G}_{glia} , with the canard on the right, while on the left, there is no saddle-node bifurcation of limit cycles for positive values of \bar{G}_{glia} (Fig.6c). It is notable that if $\bar{\varepsilon}$ or \bar{G}_{glia} are reduced from their normal values, larger amplitude oscillations in $[K]_o$ occur, whereas changing $\bar{\rho}$ results in very little change in the amplitude of the $[K]_o$ variations. Furthermore, the bistable region on the right side of the $\bar{\rho}$ diagram is quite wide, and hence hysteretic behavior as $\bar{\rho}$ is varied across this region may be amenable to experimental observation (e.g. with ouabain).

The two-parameter bifurcation diagram shown in Fig.7 provides a more complete understanding of the periodic behavior of $[K]_o$ in our reduced model with respect to the variation of $\bar{\varepsilon}$ and \bar{G}_{glia} , with $\bar{k}_{o,\infty} = 2$. The dashed lines at $\bar{G}_{glia} = 1$ and $\bar{\varepsilon} = 1$ correspond to the one-dimensional bifurcation diagrams shown in Fig.6b and 6c. The solid curves represent Hopf bifurcations, and the intersection of these dashed lines with the Hopf curves correspond to the Hopf bifurcations (points) in the earlier figures. Thus, the Hopf curves define a region within which $[K]_o$ is obliged to oscillate, because the only stable attractor is a limit cycle. To facilitate discussion, we refer to this region as the “lake of obligatory oscillation”, or LOO. Outside of the LOO, stable equilibrium solutions for $[K]_o$ exist.

The dashed line at $\bar{G}_{glia} = 1.75$ corresponds to the one-dimensional bifurcation diagram shown in Fig.8. This is drawn at the same scale as Fig.6b (the $\bar{G}_{glia} = 1$ diagram) to facilitate comparison. We note that the amplitude of the oscillation in $[K]_o$ is significantly smaller in this region of the LOO. Furthermore, the Hopf bifurcation on the right (at about $\bar{\varepsilon} = 3.2$) is now supercritical. Thus, the amplitude of the $[K]_o$ oscillation decays smoothly to zero as this point is approached from the left.

(A more complete analysis of the bifurcations present in this model will appear elsewhere.)

We now investigate whether the dynamical features identified above in our reduced model correspond to similar behavior in our full model. Fig.9 shows traces of the membrane voltage (upper traces) and $[K]_o$ (lower traces) versus time, obtained from the full model, corresponding to the parameter values marked by the numbered squares in Fig.7. For the regions outside of the LOO, the reduced model predicts stable equilibrium solutions for the ion concentrations. For example, at point 1, $[K]_o$ is slightly elevated at a value near 6mM, and the membrane voltage of the full model remains constant at -62 mV (not shown). However, at point 2, the full model exhibits tonic firing, as shown in Fig.9a. Here, $[K]_o$ is sufficiently high such that the neuron is depolarized beyond its firing threshold, and $[K]_o$ remains essentially constant with only small perturbations of order 0.1 mM due to individual spikes (Fig.9a, lower panel, see also Frankenhaeuser and Hodgkin, 1956).

Within the LOO, the reduced model predicts periodic behavior with relatively large and slow oscillations in the ion concentrations. Points 3-7 in Fig.7 correspond to Fig.9(b-f), which show various bursting behaviors of the full model. To facilitate comparison, the time scale for these figures (Fig.9b-f) is the same, showing 100 seconds of data. In addition, the voltage and concentration scales are also the same, except for the concentration scale in (b). We make the following observations from Fig.9. As the LOO is traversed from low to high $\bar{\varepsilon}$ (keeping \bar{G}_{glia} fixed) in Fig.7, the bursts become more frequent (compare Fig.9c, d; points 4, 5 and Fig.9e, f; points 6, 7). In addition, the shape of the burst envelope changes due to the decreasing amplitude of the $[K]_o$ oscillations. Note in Fig.9b (point 3) that the peak of the $[K]_o$ concentration is nearly 40mM, large enough to cause the neuron to briefly enter a state of quiescence known as “depolarization block” (see companion paper, Ullah, et al., Submitted).

Finally, we address how the location of the LOO changes with $\bar{k}_{o,\infty}$ as all other parameters are kept at their normal values. As $\bar{k}_{o,\infty}$ is increased from its normal value at 1, the LOO emerges around a value of $\bar{k}_{o,\infty} = 1.77$ as represented by the gray line on the left of Fig.10a, consistent with Rutecki, et al. (1985). As $\bar{k}_{o,\infty}$ increases the right edge of the LOO shifts towards the right, engulfing normal values of $\bar{\varepsilon}$ and \bar{G}_{glia} at (1,1), when $\bar{k}_{o,\infty}$ increased to a value of 1.9, as shown by the thick solid line (Fig.10a). As $\bar{k}_{o,\infty}$ is increased to 2.0, normal conditions for glia pumping and diffusion are well inside the LOO as shown again in Fig.10b. Fig.10c shows this oscillatory region when the reservoir concentration has been increased to 2.1. Here the left side edge of the LOO is just about to cross the point (1,1). For $\bar{k}_{o,\infty}$ greater than 2.1, oscillations in the model are only seen if either the diffusion or glial mechanisms are altered.

We conclude by reporting other possible kinds of bursting behaviors seen in our models. Fig.11a shows a time trace of the membrane voltage for $\bar{k}_{o,\infty} = 6$, $\bar{G}_{glia} = 0.1$ and $\bar{\varepsilon} = .4$. These bursts are fundamentally different from those shown in Fig.9. In particular, the extracellular potassium concentration is quite elevated, and thus the periods of quiescence correspond not to resting behavior, but rather to a state of depolarization

block. In addition, the bursts themselves have a rounded envelope, as opposed to the (approximately) square envelopes of the events in Fig.9. This behavior is consistent with the observations of Ziburkus, et al. (2006), in which interneurons were seen to enter depolarization block, giving way to pyramidal cell bursts. Bikson, et al. (2003) also observed depolarization block in pyramidal cells during electrographic seizures. We have also observed continuous “burst” firing without any quiescent intervals, as seen in Fig.11b. Here, the neuron fires continuously, but with a wavy envelope due to the oscillating ion concentrations. We include these patterns to complete the description of the possible kinds of single cell bursting behaviors seen in our models.

DISCUSSION

We have created a model which can be used to investigate the role of ion concentration dynamics on neuronal function, as well as a reduced model which is amenable to bifurcation analysis. Such bifurcations indicate major qualitative changes in system behavior, which are in many ways more predictive and informative than purely quantitative measurements. In particular we show that under otherwise normal conditions there exists a broad range of bath potassium concentration which yields seizure-like behavior in a single neuron that is both qualitatively as well as quantitatively similar to what is seen in experimental models (Feng and Durand, 2006; Mcbain et al., 1994). In fact, the values of extracellular concentration used in those experiments are quantitatively consistent with the range of concentrations shown here to exhibit seizures. Furthermore, the occurrence of stable periodic oscillations in the extracellular potassium concentration as a result of varying various experimentally and biophysically relevant parameters suggests that this may be an important mechanism underlying epileptic seizures.

In formulating our models, we made several approximations. The two most severe, insatiable glial buffering and the assumption that internal potassium can be calculated using equation (2b), should hold for times that are long compared to the time scale of individual seizures. However, for even longer times (on the order of thousands of seconds), the inevitable saturation of glia as well as decoupling of the internal potassium from the sodium dynamics will lead to more substantial errors in the calculated results. One can understand a slow saturation of the glial network as a vertical downward

drift in Fig.2. Consequently, the system may enter or leave parameter-space regions in which oscillating ion concentrations exist (e.g., see Figs.5-7). This long-term behavior could be used to more accurately model the temporal dynamics of the glial siphoning system.

It is important how the temporal potassium dynamics interacts across time scales. If the reservoir concentration, $\bar{k}_{o,\infty}$, remains only slightly elevated for a long period of time the model cell will ultimately reach a new fixed point in $[K]_o$ nearly equal to the bath concentration. This is not surprising since a stable resting state should require some degree of robustness to its micro-environment. However, as the system drifts further from the normal state we should not expect such homeostasis to persist; and the internal potassium will in general drift to higher or lower values depending on the wide variety of pumps, cotransporters, or channels inherent to the cell. When the internal potassium is integrated separately (not shown here) we see both upward and downward drift depending on model parameters as well as the initial conditions for the ionic concentrations. Therefore the seizure-like events, as well as the tonic firing reported here, are in general transient on extremely long time scales.

Although our reduced model does a good job reproducing the qualitative results of our full spiking model, there are regions where the two models disagree. These two models produce very good agreement in the region of the two-parameter graph presented in Figure 7. However the reduced model predicts the cessation of all oscillations as \bar{G}_{glia} is increased past a value of 4 (not shown), whereas the full model exhibits burst-like oscillations for far greater values. This discrepancy is due to the use of relatively simple functions used in our fitting of the time-averaged Hodgkin-Huxley currents (see Appendix A). A more sophisticated fit of these data should improve the agreement between our two models. Alternatively, a quantification of the fitting errors could be used to more precisely delineate the region in which the reduced model agrees with the full model.

Most seizures are likely due to both environmental variables as well as electrical and chemical communication between cells (not considered here; see accompanying paper, Ullah, et al., Submitted). The models presented here, however, demonstrate that

recurring seizure-like events can occur *in a single cell* that is subject to intra- and extracellular ion concentration dynamics (see also discussion in (Kager, et al., 2000) regarding single cell seizure dynamics). In particular, we have identified the basic mechanism that can give rise to such events: Hopf bifurcations in the ion concentrations.

In the companion manuscript (Ullah et al., Submitted) we discuss the effects of potassium dynamics on the stability of persistent state in networks consisting of many cells. The stability of such persistent states is related to a variety of physiological processes, which in addition to seizures, include working memory, up states, burst firing in neonatal brain and spinal cord, and perhaps spreading depression.

ACKNOWLEDGEMENTS

This work was funded by NIH Grants K02MH01493 (SJS), R01MH50006 (SJS, GU), F32NS051072 (JRC), and CRCNS-R01MH079502 (EB).

REFERENCES

- Amzica, F., Massimini, M., & Manfredi, A. (2002). A spatial buffering during slow and paroxysmal sleep oscillations in cortical networks of glial cells in vivo. *J. Neurosci.* 22:1042–1053.
- Bazhenov M, Timofeev I, Steriade M., & Sejnowski T. J. (2004). Potassium model for slow (2-3 Hz) in vivo neocortical paroxysmal oscillations. *J. Neurophysiol.* 92: 1116-1132.
- Bikson, M., Hahn, P. J., Fox, J. E., & Jefferys, J. G. R. (2003). Depolarization block of neurons during maintenance of electrographic seizures. *J. Neurophysiol.* 90(4);2402-2408.
- Dumortier, F. & Roussarie, R. (1996). Canard cycles and center manifolds. *Memoirs Am. Math. Soci.* 121(577).
- Feng, Z., & Durnad, D. M. (2006). Effects of potassium concentration on firing patterns of low-calcium epileptiform activity in anesthetized rat hippocampus: inducing of persistent spike activity. *Epilepsia.* 47(4):727-736.
- Fisher, R. S., Pedley, T. A., & Prince, D. A. (1976). Kinetics of potassium movement in norman cortex. *Brain Res.* 101(2):223-37.
- Frankenhaeuser, B., & Hodgkin, A.L. (1956). The after-effects of impulses in the giant nerve fibers of loligo. *J. Physiol.* 131:341-376.
- Gluckman B.J., Nguyen, H., Weinstein, S.L., & Schiff, S.J. (2001). Adaptive electric field control of epileptic seizures. *J. Neurosci.* 21(2):590-600.
- Heinemann, U., Lux, H. D., & Gutnick, M. J. (1977). Extracellular free calcium and potassium during paroxysmal activity in the cerebral cortex of the cat. *Exp Brain Res* 27:237–243.
- Jensen, M.S., & Yaari, Y. (1997). Role of intrinsic burs firing, potassium accumulation, and electrical coupling in the elevated potassium model of hippocampla epilepsy. *J. Neurophysiol.* 77:1224-1233.
- Lauger P. (1991). Electrogenic ion pumps. *Sunderland, MA: Sinauer.*
- Kager H, Wadman W. J., & Somjen G. G. (2000). Simulated seizures and spreading depression in a neuron model incorporating interstitial space and ion concentrations. *J. Neurophysiol.* 84: 495-512.
- Kepler T.B., Abbott, L.F., & Mardner, E. (1992). Reduction of conducatance-based neuron models. *Biol. Cybern.* 66:381-387.
- Mason, A., & Larkman, A. (1990). Correlations between morphology and electrophysiology of pyramidal neurons in slices of rat visual cortex. II. Electrophysiology. *J. Neurosci.* 10(5):1415-1428.
- Mazel, T., Simonova, Z., & Sykova, E. (1998). Diffusion heterogeneity and anisotropy in rat hippocampus. *Neuroreport.* 9(7):1299-1304.
- McBain, C. J., Traynelis, S. F., & Dingledine, R. (1990). Regional variation of extracellular space in the hippocampus. *Science.* 249(4969):674-677.
- Mcbain, C.J. (1994). Hippocampal inhibitory neuron activity in the elevated potassium model of epilepsy. *J. Neurophysiol.* 72:2853-2863.
- Moody, W. J., Futamachi, K. J., & Prince, D. A. (1974). Extracellular potassium activity during epileptogenesis. *Exp. Neurol.* 42:248–263.
- Park, E., & Durand, D.M. (2006). Role of potassium lateral diffusion in non-synaptic

- epilepsy: A computational study. *J. Theor. Biol.* 238:666-682.
- Pinsky, P.F., & Rinzel, J. (1994). Intrinsic and network rhythmogenesis in a reduced Traub model for CA3 neurons. *J. Comp. Neurosci.* 1:39-60.
- Ransom, C. B., Ransom, B. R., & Sotheimer, H. (2000). Activity-dependent extracellular K⁺ accumulation in rat optic nerve: the role of glial and axonal Na⁺ pumps. *J. Physiol.* 522:427-442.
- Rinzel, J., & Ermentrout, B. (1989). Analysis of neuronal excitability and oscillations, in "Methods in neuronal modeling: From synapses to networks", Koch, C., & Segev, I. MIT Press, revised (1998).
- Rutecki, P. A., Lebeda, F. J., & Johnston, D. (1985). Epileptiform activity induced by changes in extracellular potassium in hippocampus. *J. Neurophysiol.* 54:1363-1374.
- Scharrer, E. (1944). The blood vessels of the nervous tissue. *Quart. Rev. Biol.* 19(4):308-318.
- Somjen, G. G. (2004). Ions in the brain, *Oxford University Press, New York.*
- Traynelis, S. F., & Dingledine, R. (1988). Potassium-induced spontaneous electrographic seizures in the rat hippocampal slice. *J. Neurophysiol.* 59:259-276
- Wang, X. J. (1999). Synaptic basis of cortical persistent activity: the importance of NMDA receptors to working memory. *J. Neurosci.* 19(21):9587-9603.
- Ziburkus, J., Cressman, J. R., Barreto, E., & Schiff, S. J. (2006). Interneuron and pyramidal cell interplay during in vitro seizure-like events. *J. Neurophysiol.* 95:3948-3954.

FIGURE LEGENDS

Fig.1: Sodium potassium pump current versus extracellular potassium concentration $[K]_o$ and intracellular sodium concentration $[Na]_i$.

Fig.2: Combined glial buffering and diffusion currents as a function of the extracellular potassium concentration $[K]_o$.

Fig.3: The time averaged potassium current, $I_{K\infty}$ versus the concentration ratios $[K]_o / [K]_i$ and $[Na]_i / [Na]_o$ shown in (a), and the time averaged potassium current, $I_{K\infty}$, plotted versus the $[K]_o$ and $[Na]_i$, after the extracellular sodium and intracellular potassium have been fixed as discussed in the text (b).

Fig.4: Comparison of reduced model to the full spiking model. Top plot shows the voltage trace for a model cell. The middle traces $[K]_o$ for both the reduced model (dashed line) and full spiking model (solid line). The bottom traces show $[Na]_i$ with the same convention for the two models. All data were integrated with elevated bath concentration $\bar{k}_{o,\infty} = 2.0$, with all other parameters set to their normal values.

Fig.5: Bifurcation diagram for $[K]_o$ as a function of the bath concentration revealing a region of oscillatory behavior. All other parameters were set equal to their normal values. The filled triangles, empty triangles, filled circles, and empty circles respectively represent stable steady state, unstable steady state, stable periodic orbit, and unstable periodic orbit, in this and subsequent figures.

Fig.6: Bifurcation diagrams for $[K]_o$ as a function of the pump normalized strength (a), diffusion coefficient (b) and glial strength (c). All plots were produced under elevated extracellular bath concentration $\bar{k}_{o,\infty} = 2.0$.

Fig.7: Two dimensions bifurcation diagram for the normalized diffusion coefficient versus the glial strength. The region bounded by the black lines displays obligatory oscillatory behavior. The open circles on the Hopf curves indicate the transition from sub-critical to super-critical (i.e. Bautin bifurcations) as one progresses left to right. Time traces displaying the dynamics at the numbered points are shown in Fig.9.

Fig.8: One dimensional bifurcation diagram for $[K]_o$ oscillations as a function of the normalized diffusion coefficient. This figure was produced at an elevated bath concentration of $\bar{k}_{o,\infty} = 2.0$ and corresponds to the dashed vertical line in Fig.7 at a value of $\bar{G}_{glia} = 1.75$.

Fig.9: Time traces displaying the membrane voltage, $[K]_o$ (solid lines), and $[Na]_i$ (dashed lines) for the points depicted in Fig.7.

Fig.10: The effect of changing the bath concentration on the location of the lake of obligatory oscillations. In (a) we show two LOO's for values of $\bar{k}_{o,\infty} = 1.77$ (grey line) and $\bar{k}_{o,\infty} = 1.9$ (thick line). The plot in (b) redisplay the LOO for $\bar{k}_{o,\infty} = 2.0$, while (c) is produced at $\bar{k}_{o,\infty} = 2.1$. The square at the middle is meant to draw the eye to normal functioning glia and diffusion.

Fig.11: The behavior seen in the model for a high bath concentration, $\bar{k}_{o,\infty} = 6.0$, with reduced glial buffering $\bar{G}_{glia} = 0.1$ and diffusion $\bar{\varepsilon} = 0.4$ shown in (a). Reducing $\bar{k}_{o,\infty}$ slightly produces continuous “burst” firing without any quiescence intervals with a wavy envelop due to the oscillating ion concentrations shown in (b) – see text for further explanation.

Table 1: Model variables and parameters.

Variable	Units	Description
V	mV	Membrane potential
I_{Na}	$\mu\text{A}/\text{cm}^2$	Sodium current
I_K	$\mu\text{A}/\text{cm}^2$	Potassium current
I_L	$\mu\text{A}/\text{cm}^2$	Leak current
$m_\infty(V)$		Activating sodium gate
h		Inactivating sodium gate
n		Activating potassium gate
$\alpha(V)$		Forward rate constant for transition between open and close state of a gate
$\beta(V)$		Backward rate constant for transition between open and close state of a gate
$[Ca]_i$	mM	Intracellular calcium concentration
V_{Na}	mV	Reversal potential of persistent sodium current
V_K	mV	Reversal potential of potassium current
$[Na]_o$	mM	Extracellular sodium concentration
$[Na]_i$	mM	Intracellular sodium concentration
$[K]_o$	mM	Extracellular potassium concentration
$[K]_i$	mM	Intracellular potassium concentration
I_{pump}	mM/sec	Pump current
I_{diff}	mM/sec	Potassium diffusion to the nearby reservoir
I_{glia}	mM/sec	Glial uptake
Parameter	Value	Description
C	$1\mu\text{F}/\text{cm}^2$	Membrane capacitance
g_{Na}	$100\text{mS}/\text{m}^2$	Conductance of persistent sodium current
g_K	$40\text{mS}/\text{m}^2$	Conductance of potassium current
g_{AHP}	$0.01\text{mS}/\text{m}^2$	Conductance of afterhyperpolarization current
g_{KL}	$0.05\text{mS}/\text{m}^2$	Conductance of potassium leak current
g_{NaL}	$0.018\text{mS}/\text{m}^2$	Conductance of sodium leak current
g_{CL}	$0.05\text{mS}/\text{m}^2$	Conductance of chloride leak current
ϕ	3sec^{-1}	Time constant of gating variables
V_{Cl}	-81.93mV	Reversal potential of chloride current
g_{Ca}	$0.1\text{mS}/\text{m}^2$	Calcium conductance
V_{Ca}	120mV	Reversal potential of calcium
β	7.0	Ratio of intracellular to extracellular volume of the cell
ρ	$1.25\text{mM}/\text{sec}$	Pump strength
G_{glia}	$66\text{mM}/\text{sec}$	Strength of glial uptake
ε	1.2sec^{-1}	Diffusion constant
$k_{o,\infty}$	4.0mM	Steady state extracellular concentration
$[Cl]_o$	6.0mM	Extracellular chloride concentration
$[Cl]_i$	130.0mM	Intracellular chloride concentration

APPENDIX A

Current to concentration conversion:

In order to derive the ion concentration dynamics, we begin with the assumption that the ratio of the intracellular volume to the extracellular volume is $\beta = 7.0$ (Somjen, 2004). This corresponds to a cell with intracellular and extracellular space of 87.5% and 12.5% of the total volume respectively. For the currents across the membrane, conservation of ions requires

$$\Delta c_i Vol_i = -\Delta c_o Vol_o,$$

where c and Vol represent ion concentration and volume respectively, Δ indicates change, and the subscripts i, o correspond to the intra- and extracellular volumes. The above equation leads to

$$\Delta c_i = -\Delta c_o \left(\frac{Vol_o}{Vol_i} \right) = -\frac{\Delta c_o}{\beta}.$$

Let I be the current in units of $\mu\text{A}/\text{cm}^2$ from the Hodgkin-Huxley model. Then, the total current $i_{total} = IA$ entering the intracellular volume produces a flow of charge equal to $\Delta Q = i_{total} \Delta t$ in a time Δt , where A is membrane area. The number of ions entering the volume in this time is therefore $\Delta N = i_{total} \Delta t / q$ where q is 1.6×10^{-19} coul. The change in concentration $\Delta c_i = \Delta N / N_A Vol_i$ depends on the volume of the region to which the ions flow, where Avogadro's number N_A converts the concentration to molar. The rate of change of concentration, or concentration current $dc_i / dt = i_{c,i}$, is related to the ratio of the surface area of the cell to the volume of the cell as follows

$$i_{c,i} = \frac{\Delta c_i}{\Delta t} = \frac{\Delta N}{\Delta t Vol_i N_A} = \frac{i_{total}}{q Vol_i N_A} = \frac{IA}{q Vol_i N_A} = \frac{I}{\alpha}.$$

For a sphere of radius $7\mu\text{m}$, $\alpha = 21 \text{mCoul}/\text{M.cm}^2$. An increase in cell volume would result in a smaller time constant and therefore slower dynamics.

For the outward current the external ion concentration is therefore given as

$$i_{c,o} = \beta i_{c,i} = \frac{\beta I}{\alpha} = 0.33I$$

Equations for reduced model:

The reduced model uses empirical fits of the average membrane currents of the Hodgkin-Huxley model neuron, as described in the main text. The fits are given below.

$$I_{K\infty} = \alpha_K (g_1 g_2 g_3 + g_{IK})$$

$$I_{Na\infty} = \alpha_{Na} (g_1 g_2 g_3 + g_{INa})$$

$$K_{o/i} = [K]_o / [K]_i$$

$$Na_{i/o} = [Na]_i / [Na]_o$$

$$g_1 = 420.0(1-A_1(1-B_1 \exp(-\mu_1 Na_{i/o})))^{1/3}$$

$$g_2 = \exp(\sigma_2(1.0-\lambda_2 K_{o/i})/(1.0+\exp(-\mu_2 Na_{i/o})))$$

$$g_3 = (1/(1+\exp(\sigma_3(1.0+\mu_3 Na_{i/o} - \lambda_3 K_{o/i}))))^5$$

$$g_4 = (1/(1+\exp(\sigma_4(1.0+\mu_4 Na_{i/o} - \lambda_4 K_{o/i}))))^5$$

$$g_{IK} = A_{IK} \exp(-\lambda_{IK} K_{o/i})$$

$$g_{INa} = A_{INa}$$

where

$$\alpha_K = 1.0, \alpha_{Na} = 1.0, A_1 = .75, B_1 = .93, \mu_1 = 2.6, \lambda_2 = 7.41,$$

$$\sigma_2 = 2.0, \mu_2 = 2.6, \sigma_3 = 35.7, \mu_3 = 1.94, \lambda_3 = 24.3, \sigma_4 = .88,$$

$$\mu_4 = 1.48, \lambda_4 = 24.6, A_{INa} = 1.5, A_{IK} = 2.6, \lambda_{IK} = 32.5$$

FIGURES

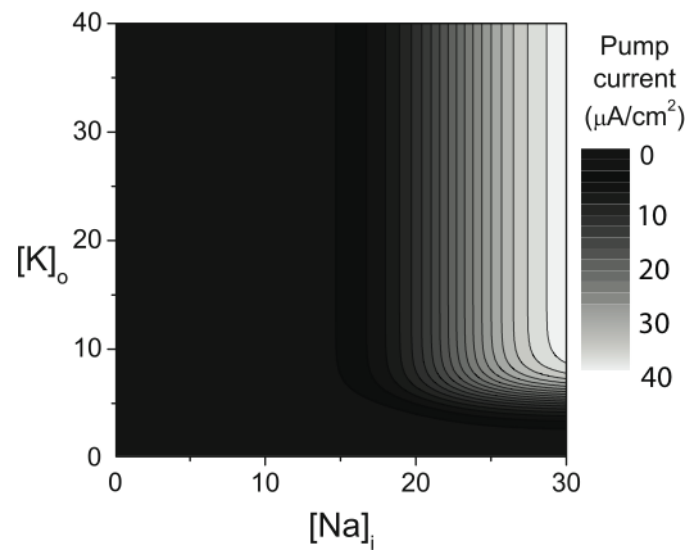


Fig. 1

FIGURES

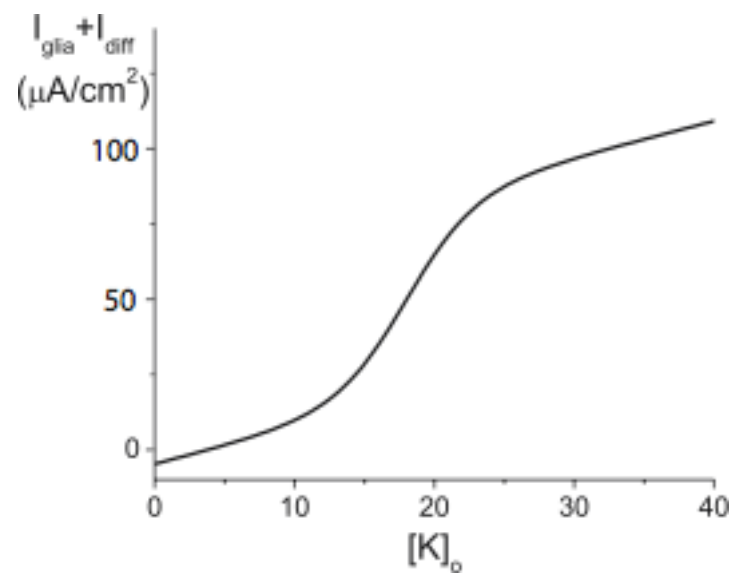


Fig.2

FIGURES

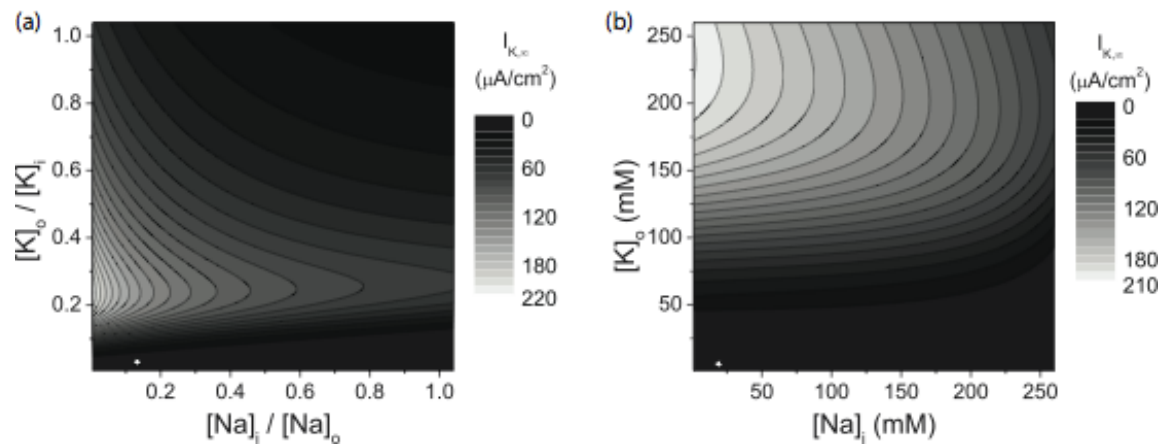


Fig. 3

FIGURES

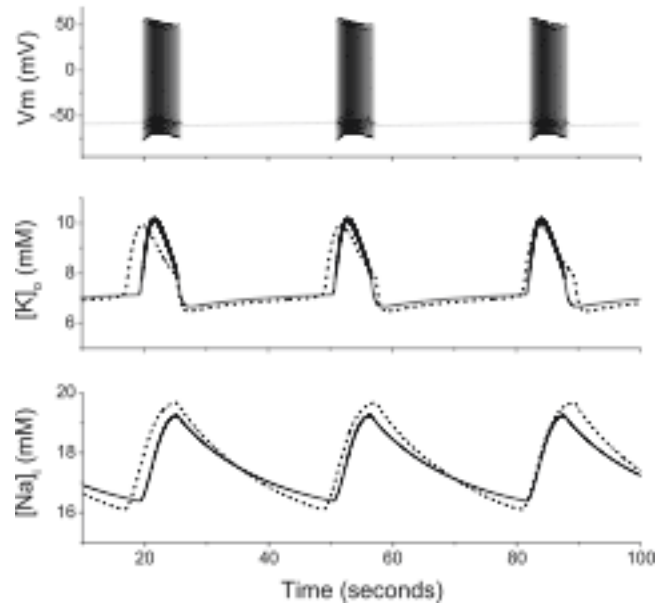


Fig. 4

FIGURES

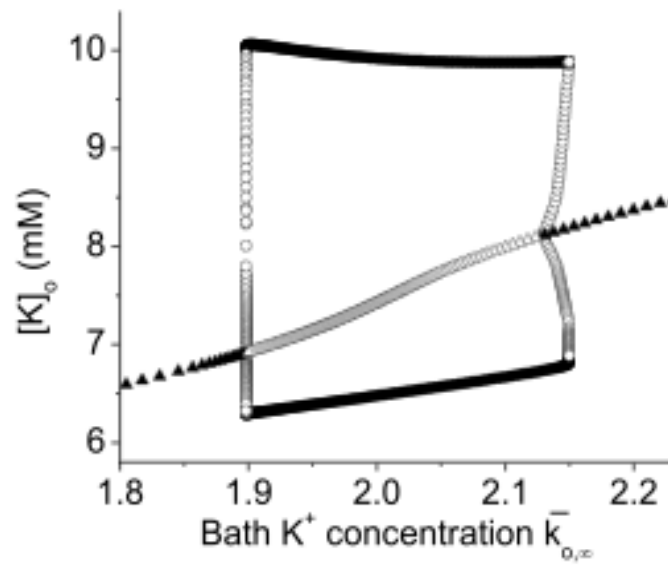


Fig. 5

FIGURES

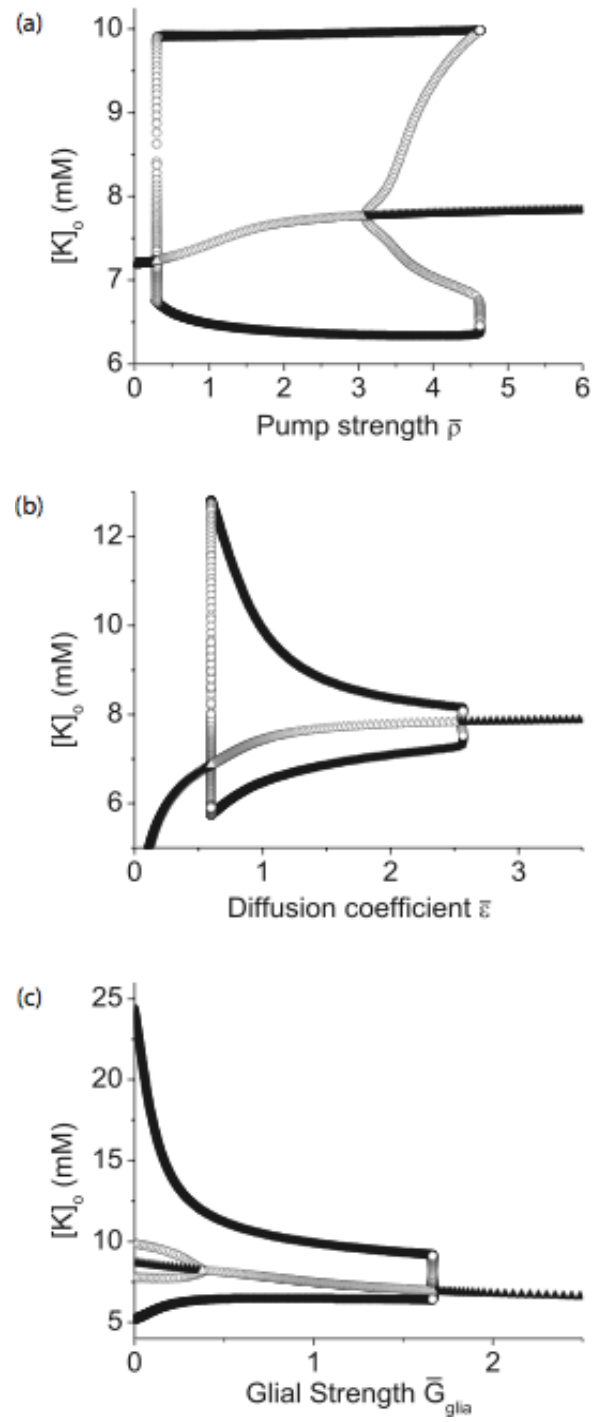


Fig. 6

FIGURES

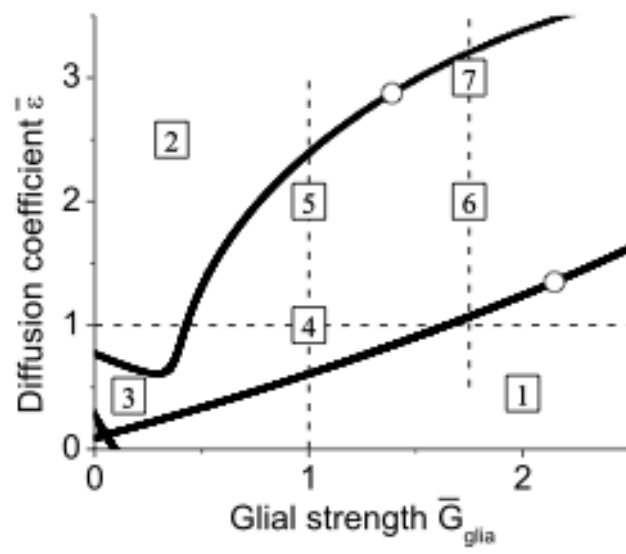


Fig. 7

FIGURES

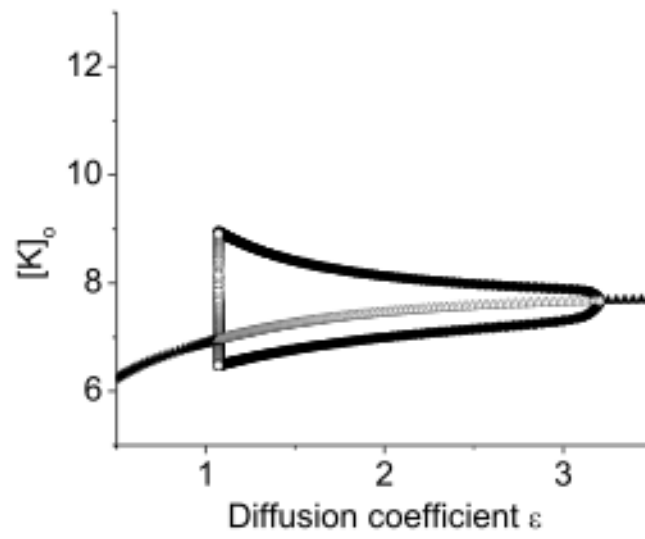


Fig. 8

FIGURES

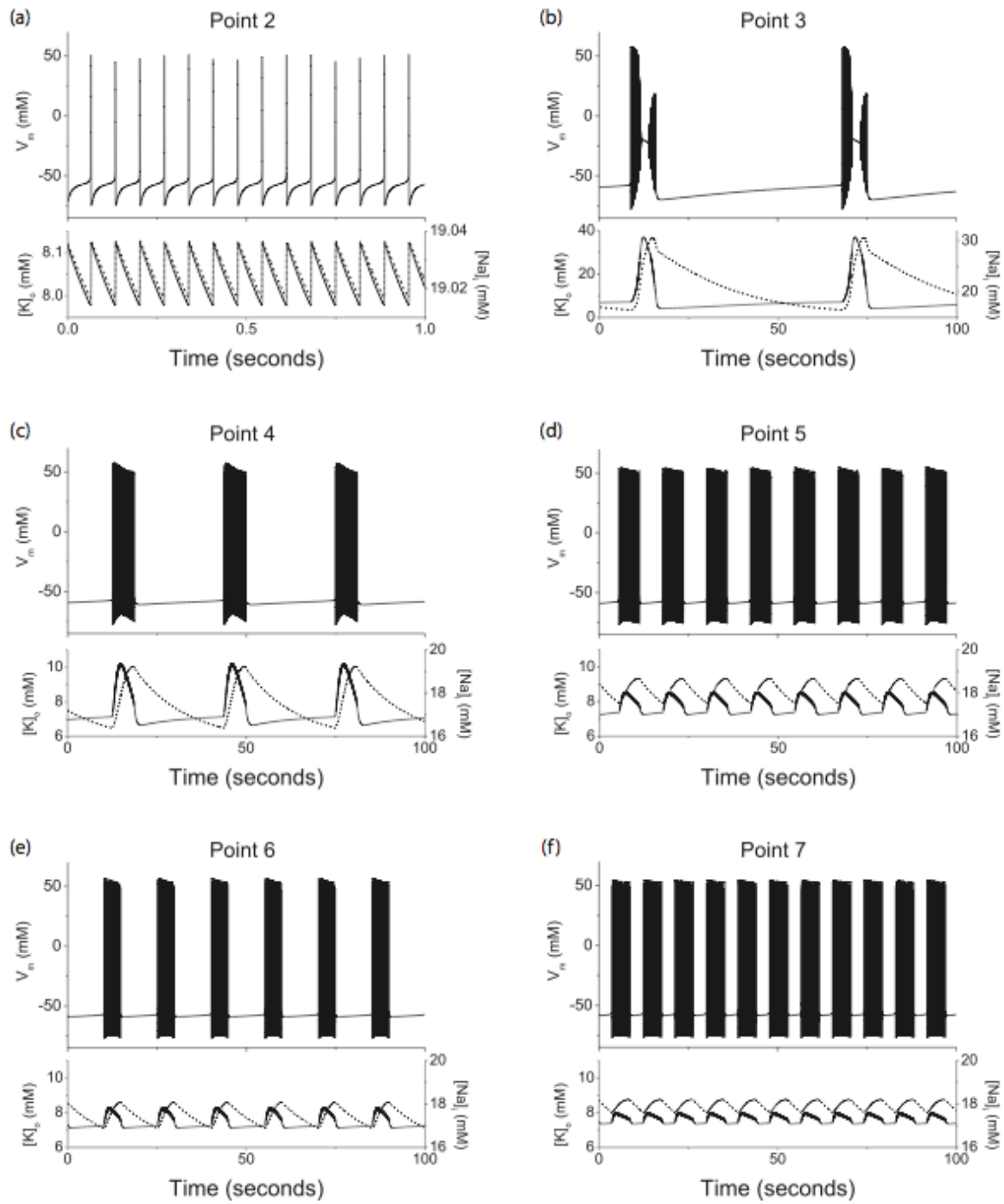


Fig. 9

FIGURES

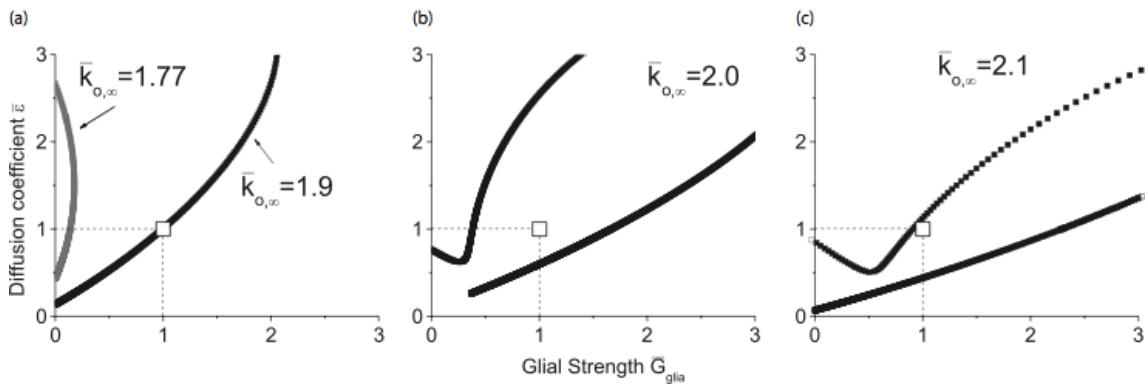


Fig. 10

FIGURES

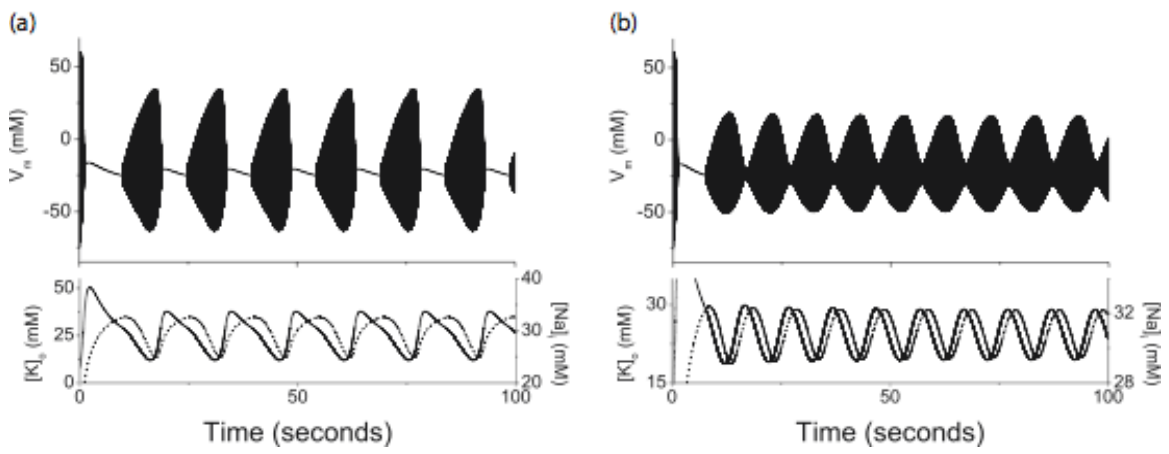


Fig. 11